THE JOURNAL OF PHYSICAL CHEMISTRY B
A JOURNAL OF THE AMERICAN CHEMICAL SOCIETY

pubs.acs.org/JPCB

Article

Structure, Thermodynamics, and Dynamics of Thiocyanate Ion Adsorption and Transfer across the Water/Toluene Interface

Ilan Benjamin*

Cite This: *J. Phys. Chem. B* 2022, 126, 5706−5714

Read Online

ACCESS | Metrics & More | Article Recommendations

ABSTRACT: Molecular dynamics simulations are used to examine in detail the structure, thermodynamics, and dynamics involve in the adsorption and transfer of the thiocyanate ion (SCN^-) across the water/toluene interface. Free energy, hydration structure, and several dynamical properties as a function of the ion location along the interface normal are calculated and contrasted with recent experiments. The free energy profile exhibits a local minimum near the interface corresponding to adsorption free energy relative to bulk water of −6 kJ/mol, in reasonable agreement with experiments. The simulations provide insight into the water surface fluctuations that are coupled to the ion transfer, demonstrating formation of water finger-like structures assisting the transfer process.

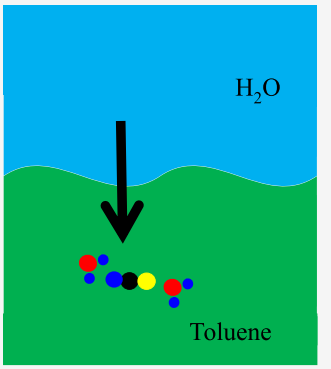

I. INTRODUCTION

Understanding the mechanism of ion transfer across the water/organic liquid interface is fundamental to many processes in environmental chemistry, nanotechnology, and electrochemistry.[1−4] This ion transfer process has been extensively studied experimentally and while many computational studies[1,4−13] have shed light on several important aspects of the mechanism of the transfer process, there are still open questions. Importantly, most theoretical studies have focused on the transfer of monatomic ions,[1,4,9−13] which typically involve large free energy of transfer. With a few exceptions,[5−8] less efforts have been invested to elucidate the process of polyatomic ions transfer. In this case, the lower free energy of transfer, the possibility of adsorption at the interface (local minima in the free energy profile) and the hydrophobic nature of some of these ions present new characteristics that could be important for both the thermodynamics and the dynamics of this process.

In this paper, we consider the relatively simple case of the interfacial adsorption and transfer of the thiocyanate anion (SCN^-) across the interface between water and toluene. Compared with previous studies on ion transfer of small ions and highly charged ions, the SCN^- ion is relatively large and not strongly hydrated (ΔG_{hyd} = −70 kcal/mol[14]). This ion plays a significant role in several important interfacial processes including the extraction of rare earth metals from aqueous to organic media[15] and several important biochemical pathways[16] and has been the focus of many surface electrochemical experiments.[1−3] Our work is also motivated by new experimental data on the adsorption of this ion at a number of water interfaces,[17−21] including the application of broad-band deep UV electronic sum-frequency generation and UV second harmonic generation to the adsorption of thiocyanate at the water/toluene interface,[21] following an earlier work utilizing resonant UV SHG to study the adsorption of this anion at the water/dodecanol interface.[18] The measured adsorption free energy of this ion and some information about its orientation serve as important validation of the molecular model we employ. There is one reported molecular dynamics simulations of the transfer of SCN^- across the water−1,2-dichloroethane interface,[22] which show a small local minima at the interface. Some of the results of that study will be contrasted with our results in the discussion below.

An important focus of the present work that did not receive detailed examination in that study is the coupling of water surface fluctuations to the transfer process. Typically, the presence of ions at water/nonpolar liquid interfaces increases the interfacial tension and decreases the interfacial width,[23] which according to capillary wave theory, reduces the amplitude of capillary waves,[24] which at the nanoscale can be viewed as water molecule protrusions. However, molecular dynamics simulations[1,9−13,25−27] and some analytical theories[28−30] of electrochemical ion transfer and assisted ion extraction at the liquid/liquid interface clearly demonstrate increased surface

Received: June 7, 2022
Revised: June 27, 2022
Published: July 21, 2022

fluctuations associated with co-transfer of water molecules, some of which are supported by experiments.[31,32] Describing the ion transfer process using generalized coordinates, which take into account surface roughness,[11,13,33] as is done below can help shed further light on this issue. We note that alternative techniques to describe the local environment of the solute as it is coupled to surface density fluctuation may be used. This includes the method of determining the instantaneous surface and describing solute properties in relation to this surface.[34,35]

The rest of this paper is organized as follows. In section II, we describe the systems, potential energy functions, and other simulation details. In section III, we discuss the results of these calculations, and in section IV, we summarize this work and present our conclusions.

II. SYSTEMS AND METHODS

II.A. System Description and Potential Energy Functions. The systems studied include a single SCN^- ion located in different locations of water/toluene interface formed by two adjacent slabs of 986 water molecules and 252 toluene molecules in a 33.6 × 33.6 × 200.0 Å rectangular box. A single sodium ion is added to the bulk water phase to obtained charge neutrality. The cation is maintained outside the SCN^- second hydration shell to minimize impact on thermodynamics and dynamics. Each liquid phase is in equilibrium with its respective vapor phase so only one liquid/liquid interface is present, located in the $X-Y$ plane at $Z \approx 0$. The water phase is in the region of $Z < 0$, and the toluene phase is in the $Z > 0$ region. Periodic boundary conditions are applied in all directions, and a reflecting wall is located 5 Å from the simulation box boundaries in the Z direction to prevent mixing of the two vapor phases.

The potential energy functions used in this work include for water a flexible version of the SPC model with intramolecular potentials of Kuchitsu and Morino[36] and for toluene a fully atomistic flexible model based on the OPLS all-atom description.[37] The intermolecular interaction potentials are represented as the pairwise sum of Lennard-Jones (LJ) and Coulomb terms:

$$u_{ij}(r) = 4\varepsilon_{ij}[(\sigma_{ij}/r)^{12} - (\sigma_{ij}/r)^{6}] + \frac{q_i q_j}{4\pi\epsilon_0 r} \quad (1)$$

where r is the distance between atom centers i and j. Standard Lorentz−Berthelot combining rules, $\sigma_{ij} = (\sigma_i + \sigma_j)/2$ and $\varepsilon_{ij} = (\varepsilon_i\varepsilon_j)^{1/2}$are used to generate LJ parameters for the interactions between atoms located in different molecules.

Because of its importance in many biological and environmental applications, considerable effort has been invested to develop accurate force fields for the interaction of the SCN^- ion with bulk water and at interfaces. We have chosen to use the recent fixed-charge model developed by Tesei *et al.*,[38] where the effect of polarizability has been incorporated by a quantum-chemical treatment of SCN^-−water interactions. This force field was shown to reproduce several experimental data including the air−water surface tension for a wide range of salt concentrations. Our SCN^- model is also fully flexible with harmonic force field parameters selected to reproduce the IR fundamental frequencies.[39]

II.B. Methods. To examine the thermodynamics, structural and dynamic properties of the SCN^- ion as a function of the distance along the interface normal, the ion is placed in $N = 40$ overlapping lamellas, each 2 Å-wide, spanning the region from bulk water to bulk toluene. In each lamella, a 5 ns constant temperature ($T = 298$ K) molecular dynamics (MD) trajectory is simulated. The ion is constrained within a specified lamella by a window potential, which is zero when the ion is inside that window but rises rapidly when the ion is outside the window. This allows for statistically accurate calculations of several structural and dynamical properties of the ion as a function of the distance from the interface. The free energy profile for the adsorption and subsequent transfer of the ion across the interface is determined using the umbrella sampling method[40−42] by combining the local free energy segments $A_n(Z)$ calculated from the ion's position probability distribution function:

$$A_n(Z) = -k_B T \ln P_n(Z),\ P_n(Z) = \langle \delta(Z - z_I) \rangle \quad (2)$$

where δ is the Dirac delta function and $P_n(Z)$ ($n = 1,2,...N$) is the ion's Z coordinate (taken as the position of the C atom) probability distribution within lamella n and the ensemble average (denoted by the triangular brackets) is calculated over all possible solvent configurations while the ion is located at $z_I = Z$. Next, the series of $A_n(Z)$ segments is combined by using their overlapping regions. All the MD simulations are performed with our in-house software that uses the velocity Verlet algorithm with an integration time step of 1 fs.

III. RESULTS AND DISCUSSION

III.A. Free Energy Profile. To note the length scale of the ion's free energy change, the density profiles of water and toluene calculated from a simulation where the SCN^- is in bulk water are shown in the top panel of Figure 1. $Z = 0$ is the location

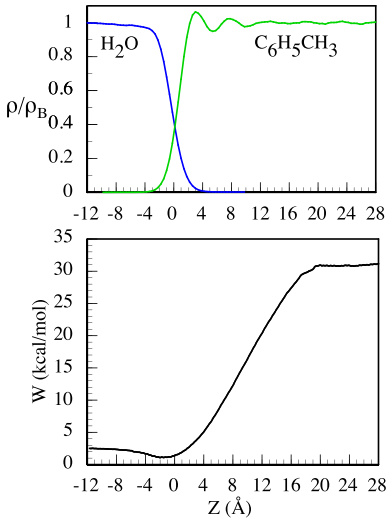

Figure 1. Top: Density profiles (relative to the respective bulk values) of water (blue) and toluene (green) at $T = 298$ K. Bottom: Free energy profile of the SCN^- ion. $Z = 0$ is the Gibbs dividing surface.

of the Gibbs dividing surface (GDS), which is the plane parallel to interface where the water density is approximately 50% of the bulk value. (For a discussion of the exact definition of the GDS, see ref 43.) The interface region (defined as the distance over which the density of water varies from 90% to 10% of the bulk value) is quite narrow at about 4 Å. However, as will be shown below, significant perturbation of the interface is observed when the ion crosses the interface.

The free energy profile for the transfer of the ion across the water/toluene interface is shown in the bottom panel of Figure

https://doi.org/10.1021/acs.jpcb.2c03956
J. Phys. Chem. B 2022, 126, 5706−5714

1. The profile exhibits a small local minimum near the GDS that corresponds to a free energy of adsorption (relative to bulk water) of about −1.4 kcal/mol (in reasonable agreement with the experimental value of −1.7 ± 0.2 kcal/mol).[21] As the ion crosses the interface, the free energy increases monotonically and reaches a plateau significantly deep into the organic phase, around Z = 20 Å. The free energy of transfer of about 27 kcal/mol is significantly smaller than the difference between the solvation free energy of the "naked" ion in toluene (estimated as −6 kcal/mol) and the hydration free energy (−70 kcal/mol[14]), suggesting that some co-transfer of first hydration water molecules is in play, as will be discussed at length below. The free energy of transfer of SCN^- across the water/DCE interface calculated using different ion interaction parameters gives a value of 17 kJ/mol,[22] that is smaller than calculated here possibly reflecting in part the higher dielectric constant of DCE.

The co-transfer of the first shell water molecules that accompany the transfer of ions from water to low dielectric organic solvent for small monovalent ions and highly charged monoatomic ions has been discussed extensively[13,44−49] but only a few studies have been published for polyatomic ions.[5,6,22] For monoatomic singly charged ions, the ability to keep a larger fraction of the first hydration shell increases as the size of the ion is reduced.[44,46] The transfer of highly charged ions involves near complete transfer of the first hydration shell. In contrast, the transfer of large hydrophobic ions involves significantly less amount of water.[11,13,49−52]

We may quantify the degree of water transfer by considering the ion−water radial distribution function as a function of the ion's position. The radial distributions functions can be calculated in each of the 40 lamellas, and in Figure 2, we show representative N−O radial distribution plots from different regions of interest, labeled by the position of the ion.

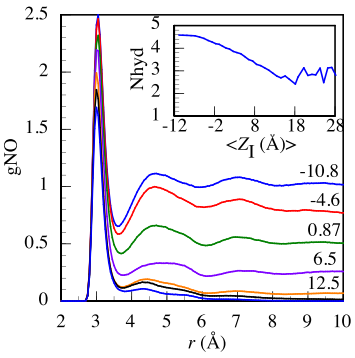

Figure 2. N−O radial distribution functions calculated when the SCN^- ion is located at different locations relative to the water/toluene Gibbs dividing surface. Each function is labeled by the average position of the SCN^-'s carbon atom when the ion is restricted to a 2 Å-wide lamella parallel to the interface. The inset shows the N atom hydration number as a function of the average ion positions for all the lamellas.

The radial distributions functions have a sharp well-defined first peak whose location remains nearly constant at 3.1 Å and a less conserved second shell structure. As expected, the asymptotic value of $g(r)$ at large r varies from 1 when the ion is in bulk water to near 0.5 when the ion is near the GDS (Z = 0) and to near zero when the ion is in bulk toluene. The height of the first peak is reduced as the ion is transferred across the interface reflecting the smaller number of water molecules in the first hydration shell. The inset in Figure 2 shows the average number of water molecules in the first hydration shell of the N atom (the smallest atom) as the SCN^- ion is transferred across the interface. The average number of water molecules in the first hydration shell N_{hyd} can be calculated from

$$N_{hyd}(r) = \int_0^{R_{min}^{(1)}} 4\pi\rho_W g(r) r^2 dr \quad (3)$$

where ρ_W is the bulk water density (0.0334 $Å^{-3}$), $g(r)$ is the O−N radial distribution function, and $R_{min}^{(1)} \approx$ 3.6 Å is the first minimum of $g(r)$. The first hydration shell number varies from 4.6 when the ion is in bulk water to near 4 as the ion crosses the interface and monotonically decrease to 3 as the ion enters deeper into the organic phase. The large fluctuations observed when Z > 18 Å reflect different relatively long-lived hydration structures that are observed once the ion completely breaks away from the aqueous phase, as will be discussed below in the section of water structure.

The "dragging" of water molecules by the ion and the monotonic diminishing of the hydration number is reflected by the average interaction energy of the SCN^- ion with the two liquids. Figure 3 shows these values as well as the interaction with first shell water molecules.

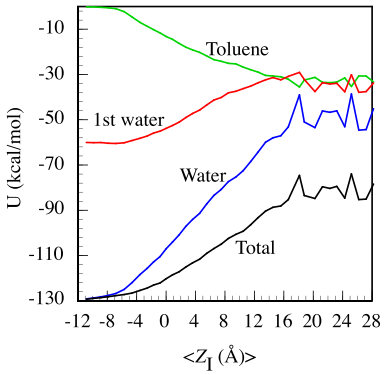

Figure 3. Average interaction energies between the SCN^- ion and the two liquids.

The decrease in the interaction energy between the first shell water molecules and the ion from about −60 kcal/mol in bulk water to −32 kcal/mol in bulk toluene corresponds to the decrease in the hydration number from 4.6 to about 3. The total water−ion interaction energy falls off more rapidly because of the more rapid decrease in the number of outer shell water molecules. As the ion enters the organic phase, its total interaction with the toluene get stronger (more negative) as there are more toluene molecules in its vicinity, but this increase is significantly more moderate than the corresponding decrease in total water−ion interactions due to the weaker electrostatic ion−toluene pair interactions. As a result, the total ion−solvent energy (black line in Figure 3) rises nearly monotonically.

III.B. Impact on Interfacial Water Structure. The co-transfer of some water molecules as the ion enters the organic phase gives rise to significant perturbation in the interfacial water structure that may significantly impact the kinetic and thermodynamics of the transfer process as well as affect other processes that may take place at the interface. Thus, it is useful to have a quantitative measure of this perturbation. A simple way to demonstrate the impact of the transferred ion on the interfacial water structure is to consider the water density profile.

https://doi.org/10.1021/acs.jpcb.2c03956
J. Phys. Chem. B 2022, 126, 5706−5714

Figure 4 demonstrates the significant coupling between the ion's location and the water density profile by showing the

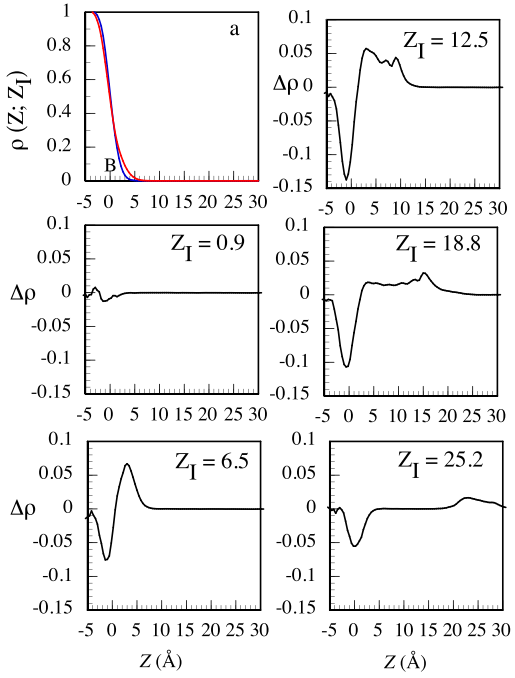

Figure 4. (a) Normalized density profile of water in the interfacial region when the ion is in bulk water (blue line labeled B) and when the ion is in some interface location (red line). The other five panels show the difference $\Delta\rho$ between the density profile of water when the ion is located at Z_I and when the ion is in bulk water.

difference $\Delta\rho = \rho\ (Z; Z_I) - \rho\ (Z;$ bulk) between the water density profile when the ion is in some (average) location Z_I and the density profile when the ion is in bulk water (which is just the neat profile). Figure 4a depicts $\rho\ (Z;$ bulk) (blueline labeled B) and (as an example) a profile for the ion in some interface location (red line). Note that each density profile is calculated in reference to the location of the GDS of that system, but since our simulation box surface area is large enough, the GDS location is almost unaffected by the location of the ion.

As the rest of the panels in Figure 4 shows, the deviation from the neat profile begins to show when the ion is near the GDS, where it rises as the ion is a few water diameters into the organic phase, reaches maximum near Z_I = 12.5 Å, and then declines when the ion is located deeper in the organic phase.

The impact on the water density profile can be summarized by computing the access number of water molecules in the organic phase relative to the normal profile: $N_{ex} = \int_{Z_{GDS}}^{Z_{BT}} \Delta\rho A dz$, where the difference between the density profiles is now in units of molecules/Å^3, where A is the simulation box cross-sectional area and the limits on the integral are from the GDS to bulk toluene (Z_{BT} is a location in the toluene phase where the water density is zero). Figure 5 shows this quantity as a function of the ion's location. (We confirmed that the N_{ex} calculated from the density profiles agrees, to within the error bars in Figure 5, with actual counting of the average excess number of water molecules relative to the neat interface.) The excess number reaches a maximum of about 13 water molecules when the ion is near 12–16 Å relative to the GDS and drops sharply to the average value of the ion's hydration number when Z_I > 18 Å. Thus, once the

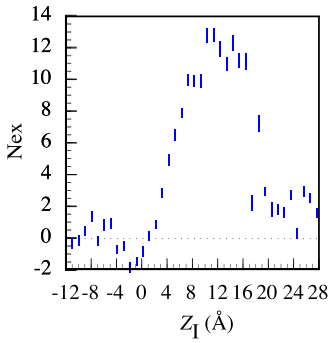

Figure 5. Average excess number of water molecules when the SCN^- ion is located at the (average) position Z_I. N_{ex} is calculated from the density profiles determined from equilibrium simulations when the single SCN^- ion is restricted to a 2 Å-wide lamella. The vertical bar represented one standard deviation in the calculated N_{ex}.

ion transfer is complete, the water structure seems to return to its equilibrium neat state.

The perturbation to the water structure caused by the ion transfer into the organic phase is in the form of water protrusions that can typically be described as a disordered single file of water molecules ("finger"). Depending on the strength of the water–ion interactions and the nature of the organic phase, this finger can be as long as a few nanometers in length before it breaks when the ion is deeper in the organic phase. The water then returns to its normal structure as the water molecules that are no longer attached to the ion via the finger retreat to the GDS region, thus explaining the maximum shown in Figure 5. Figure 6 shows an example of this finger structure.

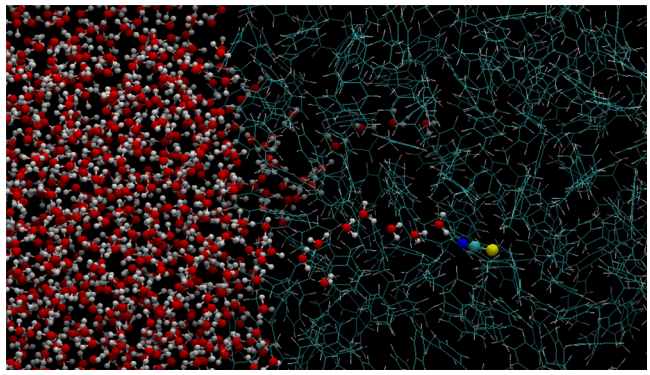

Figure 6. Snapshot showing the SCN^- ion attached to a water finger deep in the toluene phase just before a breakup.

To determine the maximum length of these water fingers as well the effective hydration state of the ion, we can use a generalized coordinate w suggested by Kikkawa *et al.*[11] To define this coordinate, the ion and water molecules are treated as vertices in an undirected graph whose edges are the geometrical distances between the vertices. A connected path between the ion and bulk water is defined by the requirement that all edges along the path are shorter than a threshold distance. The coordinate w is equal to the minimum threshold distance that will give rise to a connected path. This coordinate gives the effective separation of the ion from the water phase. More details about our implementations of the above procedure can be found elsewhere.[13,26] Here, we select the positions of the N atom (the SCN^- atom with the strongest interaction with water) and the water O atom in the above definition of the coordinate w.

https://doi.org/10.1021/acs.jpcb.2c03956
J. Phys. Chem. B 2022, 126, 5706–5714

When the ion is in bulk water, $\langle w \rangle \approx$ peak position of the N-oxygen RDF = 3.0 Å, regardless of the position Z_I of the ion. When the ion is in the organic phase connected by a water "finger" to the aqueous phase, $w \approx$ O−O distance corresponding to the longest hydrogen bond, around 3.3 Å (near the location of the first minimum of the OO radial distribution function in bulk water). After the breakup of the water "finger", w corresponds to the distance between the oxygens of the two nearest water molecules − one that belongs to the ion hydration shell and one connected to the bulk water phase. This w can be as large as values near Z_I if the interfacial water does not have any significant protrusions opposite the ion.

As the ion is deeper in the organic phase (larger Z_I values), the probability of finger breakup increases. Initial finger breakup can be permanent (on the 5 ns time scale) or it can be followed by reattachment of the finger. As an example, Figure 7 shows $w(t)$

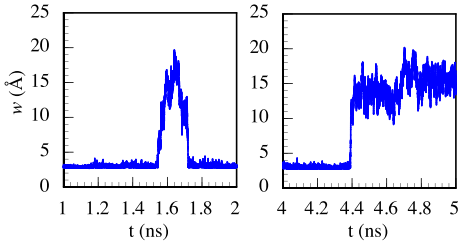

Figure 7. Water "finger" coordinate for two 1 ns segments of a trajectory with the ion constraint to a 2 Å-wide lamella centered at Z = 18 Å. The ion is connected via a water finger to the aqueous phase at t = 0.

for two 1 ns segments of the 5 ns simulation when the ion is constraint to be in the lamella centered at Z_I = 18 Å and initially (t = 0) is connected to the water phase via a water finger. The 1 ns < t < 2 ns segment shows a finger breakup that begins at $t \approx$ 1.57 ns with w reaching about 20 Å before the finger reforms at $t \approx$ 1.72 ns. The 4 ns < t < 5 ns segment shows a finger breakup that begins at $t \approx$ 4.4 ns without reforming again.

Figure 8 summarizes the results of water finger behavior as a function of the ion's location by depicting for each lamella (with

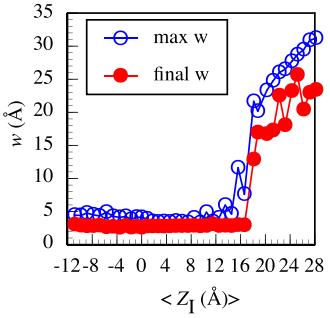

Figure 8. Maximum (open blue circles) and final (at t = 5 ns, solid red circles) values of the water finger coordinate for the ion constraint to be in a lamella vs the average location of the ion in the lamella.

the corresponding average position of the ion on the x axis) the maximum (open blue circles) and the final values (solid red circles) of w reached during the 5 ns simulation.

We can identify three regions: (a) When the ion is restricted to a lamella where the ion's average location is less than about 15 Å (relative to the GDS), the ion remains connected to the aqueous phase during the entire 5 ns trajectory; (b) when the ion average location is at 18 Å or above, the finger eventually breaks even if it may reform one or more times during the 5 ns trajectory (as shown in the example in Figure 7); (c) for the two lamellas in between these two regions, the finger breaks, reaching values near 12 and 8 Å but reform and stay connected. The transition from a fully connected finger during the entire trajectory to a region where the finger is unstable and undergoes breakup and formation before breaking again corresponds to the peak excess water in the organic phase observed in Figure 5 and also corresponds to the region when the hydration number of the ion and the interaction energy with the two solvents begin to experience significant fluctuations before they and the PMF reach a plateau. Note that $Z_I - w$ is approximately the length of an instantaneous finger, so when the ion is in the region Z_I > 24 Å and no longer connected to the aqueous phase, the length of the water finger reflects the normal fluctuations in the interfacial water density.

III.C. Solute Properties. We turn our focus now to the properties of the SCN^- ion as a function of its location relative to the interface. Some of these have been measured in bulk water and could also be measured at the interface, so the results here can be used to validate the model and offer additional insight into the effect of the interface on the ion's adsorption and transfer. The 5 ns MD equilibrium trajectory obtained in each of the 40 lamellas allows for an accurate determination of several properties characterizing the state of the ion as a function of its position along the interface normal.

Directly related to the co-transfer of water molecules with the ion across the interface and the formation of a water finger structure are the dynamics of water molecules in the hydration shell of the ion. When the ion is in bulk water, there are many water molecules outside the first hydration shell that can readily participate in an exchange with the first hydration shell, but as the ion enters the organic phase, the opportunity for exchange diminishes as there are fewer water molecules around.

Water molecule exchange dynamics between the first and second shell have been examined extensively for ions of different charge and size in bulk water,[53−56] at liquid interfaces[25] and in hydrophobic media.[26,44,46] An important characterization of this dynamics is by the average residence time of water molecules in the ion's first hydration shell. It can be determined by following the residence time correlation function:[53,54,57−59]

$$C_{res}(t) = \frac{1}{n(t)} \sum_{i=1}^{N} \langle h_i(t + t') h_i(t') \rangle \tag{4}$$

where for each distinct water molecule "i", $h_i(t)$ is equal to 1 as long as this water molecule is inside the first hydration shell. If the molecule exits for no more than some predetermined time period τ_{lag}, we keep $h_i(t)$ = 1. N is the total number of water molecules, $n(t)$ is the number of water molecules in the first hydration shell at time t, and the ensemble average is taken over all the time origins t'. The average residence time is then obtained from the time integral of $C_{res}(t)$.

The average residence time when the ion is in bulk water is quite fast, about 9 ps when calculated with τ_{lag} = 2 ps. We have confirmed that although the change in the value of τ_{lag} affects the absolute value of the residence time, it does not affect the conclusions below about the impact of the interface. Figure 9 shows that the residence time rises sharply as the ion crosses the interface and enters the organic phase and then begins to moderately drop but with large fluctuations near the region

https://doi.org/10.1021/acs.jpcb.2c03956
J. Phys. Chem. B 2022, 126, 5706−5714

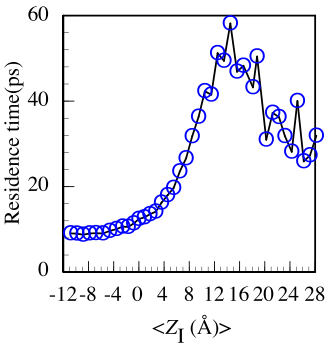

Figure 9. Average residence time of water molecules in the first hydration shell of the N atom of the SCN^- ion vs the location of the ion along the interface normal.

where the water finger reaches its maximum length before breaking up.

The initial rapid rise in the residence time correlates with the drop in the water density, as the availability of water molecules to participate in the exchange is greatly reduced when the second hydration shell is beginning to be depleted as the ion crosses the interface. As the ion leaves the GDS region on its way deeper into the organic phase, it is connected to the bulk aqueous phase by a water "finger". This further reduces the probability for water exchange and thus the residence time continue to rise. After the "finger" is broken, there is somewhat less constraint on the mobility of water molecules and there is some drop in the residence time. The increase in the residence time as the ion crosses the interface has been observed for other ion transfer cases across liquid/liquid interfaces[25] and around hydrated ions in hydrophobic media.[44,46]

An important property of ionic solute at interfaces that has not been extensively studied experimentally and theoretically (most theoretical studies involved monoatomic ions) in the context of ion transfer is molecular orientation. This property can provide significant molecular insight into the asymmetrical nature of the interface, which is relevant to understanding ion transfer. Molecular orientation can be measured using non-linear spectroscopic techniques and easily and accurately calculated. Here, we examine both the equilibrium orientational distribution and the rotational dynamics of SCN^- as a function of its location along the interface normal.

The top panel in Figure 10 shows the probability distribution for the angle θ between the interface normal and the vector pointing from the N to S atoms of the SCN^- ion. $\cos\theta = 1$ corresponds to the S atom pointing into the organic phase (the positive direction of the interface normal). As expected, the distributions are flat when the ion is in bulk water or bulk toluene. As the ion approaches the interface from the aqueous phase, there is an increased tendency for the ion to orient parallel to the interface normal with the small, higher charged N atom pointing toward the aqueous phase. The distribution becomes highly peaked as the ion gets deeper into the organic phase with the N atom connected with a water finger to the aqueous phase. While the water finger is intact, there is a significant constraint on the angular distribution (as shown in the solid black line when the average ion location is $\langle Z_I \rangle = 12.5$ Å), but once the water finger breaks (when $\langle Z_I \rangle > 18$ Å), the constraint on the ion's orientation is lifted and the distribution becomes broader and finally flat when the water finger retreats and the ion is again free to rotate.

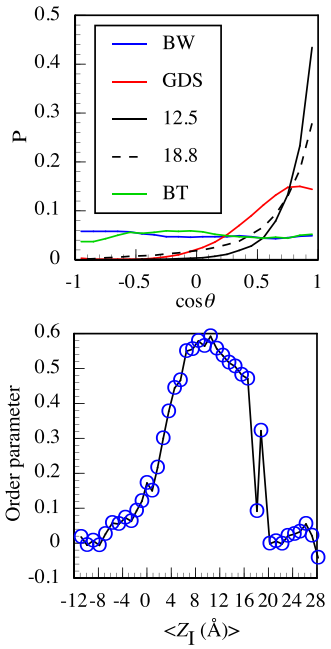

Figure 10. Top: Probability distribution for the angle θ between the normal to the interface and the vector pointing from the N to the S atoms of SCN^-. For the ion located at different positions relative to the GDS. Bottom: Orientational order parameter as a function of the ion's location relative to the GDS.

A more complete depiction of the ion orientation as a function of its location is given in the bottom panel of Figure 10 where order parameter $(3\langle\cos^2\theta\rangle - 1)/2$ (calculated from the orientational distribution function in each lamella) is plotted vs the average location of the ion. The order parameter is equal to zero when there is no orientational preference, while a value of 1 corresponds to perfect alignment along the interface normal. When the ion is at the Gibbs surface, the order parameter value is about 0.12 and $\langle\cos\theta\rangle = 0.55$ corresponds to $\theta \approx 56°$. This seems to be consistent with recent second harmonic generations experiments.[21] The sharp reversal (increase) in the order parameter near $Z_I \approx 18$ Å can be traced to an unusually stable and long-lived water finger just before breakup (see Figure 5) in a lamella that is one layer deeper into the organic phase.

We conclude with a discussion of the rotational dynamics of SCN^- as another probe of the changing environment as the ion crosses the interface and in particular its coupling to surface water structural fluctuations. The 5 ns equilibrium simulations in each of the 40 lamellas provide sufficient statistical data to accurately compute the rotational dynamics as a function of the location relative to the interface. Denoting by $\boldsymbol{u}(t)$ the unit vector pointing from the N to the S atoms of the solute at time t, we consider the following rotational time correlation function:

$$C(t) = \frac{1}{2}\{3\langle \mathbf{u}(t)\cdot\mathbf{u}(0)\rangle^2 - 1\} \tag{5}$$

where the angular brackets denote equilibrium ensemble average over all time origins. This correlation function is typically used to model the rotational anisotropy decay measured via polarization-resolved vibrational pump-probe experiments.[60]

The top panel of Figure 11 shows $C(t)$ for different solute locations (same locations used in Figure 10). Each curve can be fitted to a double exponential decay with a fast ~1 ps component nearly independent of the location and a slower component that

https://doi.org/10.1021/acs.jpcb.2c03956
J. Phys. Chem. B 2022, 126, 5706−5714

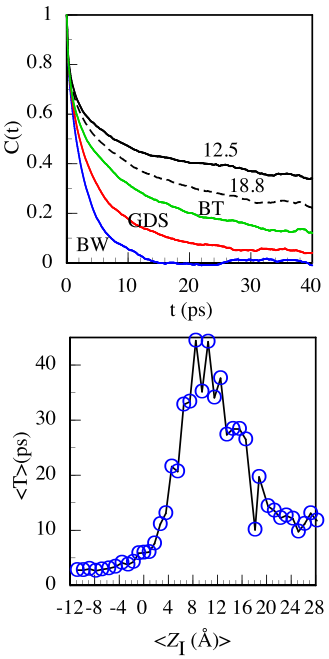

Figure 11. Top: Rotational time correlation function for the SCN^- ion in different locations. Bottom: Average rotational time as a function of the ion's location relative to the GDS.

is responsible for the observed trend. From the fit, one can obtain the average relaxation time through the relation

$$\langle T \rangle = \int_0^\infty C(t)\mathrm{d}t \tag{6}$$

The calculated rotation time in bulk water (~3.5 ps) is consistent with ultrafast IR experimental data.[61] This rotation time slowly increases as the solute approach the GDS and then rapidly rises as the solute enter the organic phase. It remains elevated while the solute is connected via the water finger to the aqueous phase since this encoring significantly reduces orientational freedom. The rotation rate drops as the finger breaks reaching a plateau at around 10 ps when the solute is in bulk toluene (but still with some water molecules in the first hydration shell). A separate independent calculation with a "dry" SCN^- in bulk toluene gives a rotation time of 2.9 ps, slightly faster than in bulk water. Clearly the three water molecules in the hydration shell of SCN^- in bulk toluene significantly slows down its rotation time. Note that within a continuum model, the rotation time of molecular ions is determined by the viscosity and dielectric constant of the liquid, as these bulk properties give rise to mechanical and dielectric frictions.[60] For a detailed discussion of the impact of solvent viscosity and dielectric properties on generic solute rotation at liquid/liquid interface, see ref 62. At the molecular scale, the rotation time is better understood in terms of the solute−solvent intermolecular interactions and the impact of the solute on the water hydrogen bonding network. The relatively rapid rotation of SCN^- in bulk water is related to the ion's ability to efficiently switch hydrogen bonding partners with water molecules as is also evident in the rapid water exchange dynamics discussed earlier. The inadequacy of continuum models to explain surface effects is clearly evident from the data presented above: The surface effect observed here is entirely due to the unique surface structural fluctuations magnified by the presence of the ion.

IV. SUMMARY AND CONCLUSIONS

The study via MD simulations of the adsorption and transfer of the thiocyanate ion across the water/toluene interface provides new insight into the structural and dynamical factors influencing polyatomic ion transfer across the interface. The relatively (weak) hydrophilic nature of the ion results in a local free energy at the interface corresponding to an adsorption free energy of −6 kJ/mol, in reasonable agreement with experiments. Despite the relatively weak interactions between the ion and bulk water relative to that of smaller hydrophilic monoatomic ions whose transfer has been extensively studied, the transfer of this ion into a very low dielectric constant medium involves significant dragging of water molecules in the form of water fingers. As the ion location is varied from bulk water across the interface to bulk toluene, the variation in a number of properties such as water excess in the organic phase, solute orientation and orientational dynamics, and water molecule residence time in the ion's first hydration shell exhibits a non-monotonic behavior. It is shown that this behavior is directly correlated with the formation an eventual breakdown of the water finger-like structure.

AUTHOR INFORMATION

Corresponding Author

Ilan Benjamin − *Department of Chemistry and Biochemistry, University of California, Santa Cruz, California 95064, United States;* orcid.org/0000-0003-0056-4925; Email: ilan@ucsc.edu

Complete contact information is available at: https://pubs.acs.org/10.1021/acs.jpcb.2c03956

Notes

The author declares no competing financial interest.

ACKNOWLEDGMENTS

Many thanks for the Saykally group for sharing experimental data and for helpful discussions. Financial support from the National Science Foundation through grant CHE-1800158 is acknowledged.

REFERENCES

(1) Dryfe, R. A. W. The Electrified Liquid-Liquid Interface. *Adv. Chem. Phys.* **2009**, *141*, 153−215.
(2) Vallejo, L. J. S.; Ovejero, J. M.; Fernandez, R. A.; Dassie, S. A. Simple Ion Transfer at LiquidlLiquid Interfaces. *Int. J. Electrochem.* **2012**, *2012*, 1−34.
(3) Benjamin, I. Reaction Dynamics at Liquid Interfaces. *Annu. Rev. Phys. Chem.* **2015**, *66*, 165−188.
(4) Morita, A.; Koizumi, A.; Hirano, T. Recent progress in simulating microscopic ion transport mechanisms at liquid-liquid interfaces. *J. Chem. Phys.* **2021**, *154*, 080901−080908.
(5) Schweighofer, K. J.; Benjamin, I. Transfer of a tetra methyl ammonium ion across the water-nitrobenzene interface: Potential of mean force and non-equilibrium dynamics. *J. Phys. Chem. A* **1999**, *103*, 10274−10279.
(6) Benjamin, I. Recombination, Dissociation and Transport of Ion Pairs Across the Liquid/Liquid Interface. Implications for Phase Transfer Catalysis. *J. Phys. Chem. A* **2013**, *117*, 4325−4331.
(7) Luo, G.; Malkova, S.; Yoon, J.; Schultz, D. G.; Lin, B.; Meron, M.; Benjamin, I.; Vanysek, P.; Schlossman, M. L. Ion Distributions Near a Liquid-Liquid Interface. *Science* **2006**, *311*, 216.
(8) Liang, Z.; Bu, W.; Schweighofer, K. J.; Walwark, D. J., Jr.; Harvey, J. S.; Hanlon, G. R.; Amoanu, D.; Erol, C.; Benjamin, I.; Schlossman, M. L. Nanoscale view of assisted ion transport across the liquid-liquid interface. *Proc. Natl. Acad. Sci. U. S. A.* **2018**, *116*, 18227−18232.

(9) Benjamin, I. Molecular structure and dynamics at liquid-liquid interfaces. *Annu. Rev. Phys. Chem.* **1997**, *48*, 407−451.
(10) Chang, T. M.; Dang, L. X. Recent advances in molecular simulations of ion solvation at liquid interfaces. *Chem. Rev.* **2006**, *106*, 1305−1322.
(11) Kikkawa, N.; Wang, L. J.; Morita, A. Microscopic Barrier Mechanism of Ion Transport through Liquid-Liquid Interface. *J. Am. Chem. Soc.* **2015**, *137*, 8022−8025.
(12) Benjamin, I. Reactivity and Dynamics at Liquid Interfaces. *Rev. Comput. Chem.* **2015**, *28*, 205−313.
(13) Karnes, J. J.; Benjamin, I. Geometric and energetic considerations of surface fluctuations during ion transfer across the water-immiscible organic liquid interface. *J. Chem. Phys.* **2016**, *145*, 014701−014707.
(14) Marcus, Y., *Ions In Solution And Their Solvation*. Wiley: Hoboken, New Jersey, 2015.
(15) Lovering, K.; Nayak, S.; Bu, W.; Uysal, A. The Role of Specific Ion Effects in Ion Transport: The Case of Nitrate and Thiocyanate. *J. Phys. Chem. C* **2020**, *124*, 573−581.
(16) Pedemonte, N.; Caci, E.; Sondo, E.; Caputo, A.; Rhoden, K.; Pfeffer, U.; Di Candia, M.; Bandettini, R.; Ravazzolo, R.; Zegarra-Moran, O.; Galietta, L. J. Thiocyanate transport in resting and IL-4-stimulated human bronchial epithelial cells: role of pendrin and anion channels. *J. Immunol.* **2007**, *178*, 5144−5153.
(17) Petersen, P. B.; Saykally, R. J.; Mucha, M.; Jungwirth, P. Enhanced concentration of polarizable anions at the liquid water surface: SHG spectroscopy and MD simulations of sodium thiocyanide. *J. Phys. Chem. B* **2005**, *109*, 10915−10921.
(18) Onorato, R. M.; Otten, D. E.; Saykally, R. J. Adsorption of thiocyanate ions to the dodecanol/water interface characterized by UV second harmonic generation. *Proc. Natl. Acad. Sci. U. S. A.* **2009**, *106*, 15176−15180.
(19) Otten, D. E.; Shaffer, P. R.; Geissler, P. L.; Saykally, R. J. Elucidating the mechanism of selective ion adsorption to the liquid water surface. *Proc. Natl. Acad. Sci. U. S. A.* **2012**, *109*, 701−705.
(20) McCaffrey, D. L.; Nguyen, S. C.; Cox, S. J.; Weller, H.; Alivisatos, A. P.; Geissler, P. L.; Saykally, R. J. Mechanism of ion adsorption to aqueous interfaces: Graphene/water vs. air/water. *Proc. Natl. Acad. Sci.* **2017**, *114*, 13369−13373.
(21) Devlin, S. W.; McCaffrey, D. L.; Saykally, R. J. Characterizing Anion Adsorption to Aqueous Interfaces: Toluene-Water versus Air-Water. *J. Phys. Chem. Lett.* **2022**, *13*, 222−228.
(22) Darvas, M.; Jorge, M.; Cordeiro, M. N. D. S.; Jedlovszky, P. Solvation Free Energy Profile of the SCN- Ion across the Water-1,2-Dichloroethane Liquid/Liquid Interface. A Computer Simulation Study. *J. Phys. Chem. C* **2011**, *115*, 11140−11146.
(23) Adamson, A. W., *Physical Chemistry of Surfaces*; Fifth ed. Wiley: New York, 1990.
(24) Rowlinson, J. S.; Widom, B., *Molecular Theory of Capillarity*. Clarendon: Oxford, 1982.
(25) Chorny, I.; Benjamin, I. Hydration shell exchange dynamics during ion transfer across the liquid/liquid interface. *J. Phys. Chem. B* **2005**, *109*, 16455−16462.
(26) Benjamin, I. Hydronium ion at the water/1,2-dichloroethane interface: Structure, thermodynamics, and dynamics of ion transfer. *J. Chem. Phys.* **2019**, *151*, No. 094701.
(27) Kumar, N.; Servis, M.; Liu, Z.; Clark, A. E. Competitive Interactions at Electrolyte/Octanol Interfaces: A Molecular Perspective. *J. Phys. Chem. C* **2020**, *124*, 10924−10934.
(28) Marcus, R. A. On the theory of ion transfer rates across the interface of two immiscible liquids. *J. Chem. Phys.* **2000**, *113*, 1618−1629.
(29) Kornyshev, A. A.; Kuznetsov, A. M.; Urbach, M. Coupled ion-interface dynamics and ion transfer across the interface of two immiscible liquids. *J. Chem. Phys.* **2002**, *117*, 6766−6779.
(30) Verdes, C. G.; Urbakh, M.; Kornyshev, A. A. Surface tension and ion transfer across the interface of two immiscible electrolytes. *Electrochem. Commun.* **2004**, *6*, 693−699.
(31) Osakai, T.; Ogata, A.; Ebina, K. Hydration of ions in organic solvent and its significance in the Gibbs energy of ion transfer between two immiscible liquids. *J. Phys. Chem. B.* **1997**, *101*, 8341−8348.
(32) Osakai, T., The role of water molecules in ion transfer at the oil/water interface. In *Interfacial Catalysis*; Volkov, A. G., Ed. Marcel Dekker: New York, 2002; pp. 53−82.
(33) Kikkawa, N.; Wang, L.; Morita, A. Computational study of effect of water finger on ion transport through water-oil interface. *J. Chem. Phys.* **2016**, *145*, No. 014702.
(34) Willard, A. P.; Chandler, D. Instantaneous Liquid Interfaces. *J. Phys. Chem. B* **2010**, *114*, 1954−1958.
(35) Jorge, M.; Hantal, G.; Jedlovszky, P.; Cordeiro, M. N. D. S. Critical Assessment of Methods for the Intrinsic Analysis of Liquid Interfaces: 2. Density Profiles. *J. Phys. Chem. C* **2010**, *114*, 18656−18663.
(36) Kuchitsu, K.; Morino, Y. Estimation of anharmonic potential constants. II. Bent XY2 molecules. *Bull. Chem. Soc. Jpn.* **1965**, *38*, 814−824.
(37) Damm, W.; Frontera, A.; TiradoRives, J.; Jorgensen, W. L. OPLS all-atom force field for carbohydrates. *J. Comput. Chem.* **1997**, *18*, 1955−1970.
(38) Tesei, G.; Aspelin, V.; Lund, M. Specific Cation Effects on SCN^- in Bulk Solution and at the Air-Water Interface. *J. Phys. Chem. B* **2018**, *122*, 5094−5105.
(39) Jones, L. H. Infrared Spectrum and Structure of the Thiocyanate Ion. *J. Chem. Phys.* **1956**, *25*, 1069−1072.
(40) Allen, M. P.; Tildesley, D. J., *Computer Simulation of Liquids*. Clarendon: Oxford, 1987.
(41) Kumar, S.; Rosenberg, J. M.; Bouzida, D.; Swendsen, R. H.; Kollman, P. A. Multidimensional Free-Energy Calculations Using the Weighted Histogram Analysis Method. *J. Comput. Chem.* **1995**, *16*, 1339−1350.
(42) Kastner, J. Umbrella sampling. *WIREs Comput. Mol. Sci.* **2011**, *1*, 932−942.
(43) Rowlinson, J. S.; Widom, B., *Molecular Theory of Capillarity*; Clarendon: Oxford, 1982; p 115.
(44) Benjamin, I. Structure and dynamics of hydrated ions in a water-immiscible organic solvent. *J. Phys. Chem. B* **2008**, *112*, 15801−15806.
(45) Rose, D.; Benjamin, I. Free energy of transfer of hydrated ion clusters from water to an immiscible organic solvent. *J. Phys. Chem. B* **2009**, *113*, 9296−9303.
(46) Benjamin, I. Molecular dynamics study of hydrated alkali and halide ions in liquid nitrobenze. *J. Electroanal. Chem.* **2010**, *650*, 41−46.
(47) Jungwirth, P.; Tobias, D. J. Specific ion effects at the air/water interface. *Chem. Rev.* **2006**, *106*, 1259−1281.
(48) Wick, C. D.; Dang, L. X. Molecular dynamics study of ion transfer and distribution at the interface of water and 1,2-dichlorethane. *J. Phys. Chem. C* **2008**, *112*, 647−649.
(49) Karnes, J. J.; Villavicencio, N.; Benjamin, I. Transfer of an erbium ion across the water/dodecane interface: Structure and thermodynamics via molecular dynamics simulations. *Chem. Phys. Lett.* **2019**, *737*, 136825−136830.
(50) Benjamin, I. Mechanism and dynamics of ion transfer across a liquid-liquid interface. *Science* **1993**, *261*, 1558−1560.
(51) Wick, C. D.; Dang, L. X. Molecular dynamics study of ion transfer and distribution at the interface of water and 1,2-dichlorethane. *J. Phys. Chem. C* **2008**, *112*, 647−649.
(52) Qiao, B. F.; Muntean, J. V.; de la Cruz, M. O.; Ellis, R. J. Ion Transport Mechanisms in Liquid-Liquid Interface. *Langmuir* **2017**, *33*, 6135−6142.
(53) Koneshan, S.; Rasaiah, J. C.; Lynden-Bell, R. M.; Lee, S. H. Solvent Structure, Dynamics, and Ion Mobility in Aqueous Solutions at 25 °C. *J. Phys. Chem. B* **1998**, *102*, 4193−4204.
(54) Laage, D.; Hynes, J. T. On the Residence Time for Water in a Solute Hydration Shell: Application to Aqueous Halide Solutions. *J. Phys. Chem. B.* **2008**, *112*, 7697−7701.
(55) Lee, S. H.; Rasaiah, J. C. Molecular dynamics simulation of ionic mobility. 2. Alkali metal and Halide ions using the SPC/E model for water at 25°C. *J. Phys. Chem.* **1996**, *100*, 1420−1425.

https://doi.org/10.1021/acs.jpcb.2c03956
J. Phys. Chem. B 2022, 126, 5706−5714

(56) Roy, S.; Dang, L. X. Water exchange dynamics around H_3O^+ and OH^- ions. *Chem. Phys. Lett.* **2015**, *628*, 30−34.
(57) Impey, R. W.; Madden, P. A.; McDonald, I. R. Hydration and mobility of ions in solution. *J. Phys. Chem.* **1983**, *87*, 5071−5083.
(58) Lee, S. H.; Rossky, P. J. A comparison of the structure and dynamics of liquid water at hydrophobic and hydrophilic surfaces - a molecular-dynamics simulation study. *J. Chem. Phys.* **1994**, *100*, 3334−3345.
(59) Bizzarri, A. R.; Cannistraro, S. Molecular Dynamics of Water at the Protein-Solvent Interface. *J. Phys. Chem. B* **2002**, *106*, 6617−6633.
(60) Fleming, G. R., *Chemical Applications of Ultrafast Spectroscopy*; Oxford University: New York, 1986.
(61) Bian, H. T.; Chen, H. L.; Zhang, Q.; Li, J. B.; Wen, X. W.; Zhuang, W.; Zheng, J. R. Cation Effects on Rotational Dynamics of Anions and Water Molecules in Alkali (Li^+, Na^+, K^+, Cs^+) Thiocyanate (SCN^-) Aqueous Solutions. *J. Phys. Chem. B* **2013**, *117*, 7972−7984.
(62) Benjamin, I. Solute Orientational Dynamics at the Water/Carbon Tetrachloride Interface. *J. Phys. Chem. C* **2008**, *112*, 8969−8975.

https://doi.org/10.1021/acs.jpcb.2c03956
J. Phys. Chem. B 2022, 126, 5706−5714